PCCP

PAPER

View Article Online
View Journal | View Issue

Cite this: *Phys. Chem. Chem. Phys.*, 2014, **16**, 5142

Complexes containing CO_2 and SO_2. Mixed dimers, trimers and tetramers†

Luis Miguel Azofra[ab] and Steve Scheiner*[b]

Received 28th December 2013,
Accepted 24th January 2014

DOI: 10.1039/c3cp55489a

www.rsc.org/pccp

Mixed dimers, trimers and tetramers composed of SO_2 and CO_2 molecules are examined by *ab initio* calculations to identify all minimum energy structures. While AIM formalism leads to the idea of a pair of C···O bonds in the most stable heterodimer, bound by some 2 kcal mol^{-1}, NBO analysis describes the bonding in terms of charge transfer from O lone pairs of SO_2 to the CO π* antibonding orbitals. The second minimum on the surface, just slightly less stable, is described by AIM as containing a single O···O chalcogen bond. The NBO picture is that of two transfers in opposite directions: one from a SO_2 O lone pair to a π* antibond of CO_2, supplemented by CO_2 $O_{lp} \rightarrow \pi^*(SO)$. Decomposition of the interaction energies points to electrostatic attraction and dispersion as the dominant attractive components, in roughly equal measure. The various heterotrimers and tetramers generally retain the dimer structure as a starting point. Cyclic oligomers are favored over linear geometries, with a preference for complexes containing larger numbers of SO_2 molecules.

Introduction

Noncovalent interactions between molecules are central to condensed phases and to our understanding of the structures adopted by a wide range of single molecules such as proteins and nucleic acids. There is an assortment of different noncovalent forces, among which the hydrogen bond (HB) has been intensively studied over a long period of time.[1–4] Earlier ideas about the nature of HBs in which the proton donor and acceptor atoms are F, O, or N has slowly been modernized to a more generalized scheme which includes less electronegative atoms like Cl, S, or C,[5–9] and the idea that the bridging proton interacts with a lone electron pair has been extended to π and σ bonds,[10–14] and even to a hydridic H atom within the context of dihydrogen bonds.[12,15–18]

A different but related class of noncovalent bond is associated with the attraction between a pair of electronegative atoms. Depending upon the nature of the bridging atom, these interactions are commonly designated as halogen,[19–24] chalcogen,[25–31] or pnicogen[23,32–41] bonds. The attractive force has been attributed to an anisotropic distribution of electron density around the bridging X atom, characterized by a crown of positive electrostatic potential along the extension of the Y–X bond (σ-hole) or in areas perpendicular to it (π-hole).[42–46] This latter region is attracted to the partial negative charge of a neighboring molecule. Like HBs, the electrostatic attractions within these bonds are supplemented by charge transfer from the lone pair(s) of the acceptor atom into the σ* or π* antibonding Y–X orbitals, respectively, which tends to weaken and lengthen the latter Y–X bond. Attractive London (dispersion) forces further supplement the overall binding energy.

Attractive forces between stacked aromatic systems served as a springboard to examine other noncovalent bonds which are dominated by $\pi \rightarrow \pi^*$ charge transfers. As an example, it was recently shown[47] that a pair of amide units can arrange themselves in a stacked configuration with almost the same binding energy as the standard NH···O HBs that are a hallmark of α-helices and β-sheets in proteins. A dominant contributor to this stacked geometry is the transfer of charge from the CO π bond of one amide to the CO π* antibond of its neighbor, an idea that has been reinforced by others.[48] There are other related systems which have been proposed to be held together in part by transfers into a π* antibond, with the charge originating in a lone pair of the partner molecule.[49–52]

We have recently examined the interesting sorts of interactions that arise when SO_2 is paired with H_2CO and H_2CS, not only as dimers, but also in larger aggregates.[53] These molecules were bound together by surprisingly strong forces, exceeding 5 kcal mol^{-1}. The noncovalent bonds were identified as CH···O HBs and S···O chalcogen bonds, the latter of which was characterized by charge transfer from an O lone pair to a S–O π* antibonding orbital. An even more unusual sort of bond arose from the charge transfer from a SO_2 oxygen lone pair to the C–S π* antibonding orbital of H_2CS.

[a] *Instituto de Química Médica, CSIC, Juan de la Cierva, 3, E-28006, Madrid, Spain*
[b] *Department of Chemistry and Biochemistry, Utah State University, Logan, UT 84322-0300, USA. E-mail: steve.scheiner@usu.edu; Fax: +1-435-797-3390*

† Electronic supplementary information (ESI) available. See DOI: 10.1039/c3cp55489a

In the present work, we consider the interactions between CO_2 and its SO_2 congener. The first molecule is of particular interest in that its linear geometry imbues it with a zero dipole moment, which cuts down on Coulombic interactions. The absence of H atoms also precludes the presence of any HBs, even in a secondary role. The binding here is thus reduced, but is nonetheless substantial, in the neighborhood of 2 kcal mol^{-1}. The analysis reveals the attraction is due primarily to transfers from the O lone pair to the antibonding π^* orbitals, of both CO and SO type. Analysis of trimers and tetramers provides an estimate of the influence of cooperative effects in stabilizing larger aggregates, and in determining the origin of the attractive forces, some of which are not present in the simpler dimers.

From a more practical standpoint, both CO_2 and SO_2 have relevance in a number of fields such as biological, industrial and environmental chemistry. CO_2 is a main product of cellular respiration and also of the carbon combustion that contributes so heavily to the greenhouse effect.[54] In that sense, its role in climate change is a topic of current and growing interest. Furthermore, supercritical carbon dioxide (sc-CO_2) has been the subject of research involving so-called green solvents,[55] *i.e.*, solvents that have minimal environmental impact (cost, safety and health issues). Experimental work has been aimed toward greater understanding of the behavior of sc-CO_2 as solvent with organic compounds.[56] From another direction, computational efforts have added to understanding the role of the CO_2-philicity with different solutes, as for example, peracetylated β-cyclodextrins,[57] and carbonyl[58] and carbamides[59] (as simple models of aminoacids) derivatives. SO_2 is a principal cause of acid rain,[60] due to its ability to form SO_3 which in combination with water, leads to the formation of sulfuric acid. The reaction of carbonyl oxides with SO_2 is also relevant, due to the possible contribution of this reaction to acid rain, which was experimentally studied in the 1980s by Calvert *et al.*[61]

Computational methods

The geometries and properties of the CO_2:SO_2 heterodimers, the CO_2:$(SO_2)_2$ and $(CO_2)_2$:SO_2 heterotrimers, and the CO_2:$(SO_2)_3$ and $(CO_2)_3$:SO_2 heterotetramers were optimized and analyzed through the use of the second-order Møller–Plesset perturbation theory (MP2)[62] with the aug-cc-pVDZ basis set.[63–66] In all cases, vibrational frequencies were calculated in order to confirm that the structures correspond to true minima and to obtain the zero point vibrational energy (ZPE). Also, single-point CCSD(T)[67]/aug-cc-pVTZ calculations were performed for the CO_2:SO_2 heterodimers, using MP2/aug-cc-pVDZ optimized geometries so as to obtain more accurate values. All these calculations were performed with the GAUSSIAN09 program.[68]

Interaction energies, E_{int}, were computed as the difference in energy between the binary complex on one hand, and the sum of the energies of the two monomers on the other, using the monomer geometries from the optimized complex. Interaction energies for the heterodimers were corrected by the counterpoise procedure.[69] In addition, binding energies, E_b, were computed as the difference in energy between the complex on one hand, and the sum of the energies of the optimized monomers on the other, taking into account also the ZPE. The multi-body procedure was applied to trimers (eqn (1)) and tetramers (eqn (2)), whereby the interaction energy can be expressed as:

$$E_{int}\ (\text{trimer}) = \Sigma\Delta^2E + \Delta^3E \quad (1)$$

$$E_{int}\ (\text{tetramer}) = \Sigma\Delta^2E + \Sigma\Delta^3E + \Delta^4E \quad (2)$$

where Δ^nE is the n^{th} complex term (2 = for dimers, 3 = for trimers, *etc.*) and the largest value of n represents the total cooperativity in the full complex.

Further analysis was carried out *via* the Atoms in Molecules (AIM)[70] approach at the MP2-level using the AIMAll program,[71] and Natural Bond Orbital (NBO)[72] treatment with the ωB97XD[73] functional, using the NBO6.0 program.[74] The interaction energy of each CO_2:SO_2 heterodimer was decomposed *via* DFT-SAPT calculations at the PBE0[75]/aug-cc-pVTZ level with the MOLPRO program.[76] The DFT-SAPT interaction energy, $E^{DFT\text{-}SAPT}$, is obtained as the sum of five components (eqn (3)): electrostatic (E_{ele}), exchange (E_{exc}), induction (E_{ind}), dispersion (E_{dis}) and higher-order contributions (δ_{HF}).[77]

$$E^{DFT\text{-}SAPT} = E_{ele} + E_{exc} + E_{ind} + E_{dis} + \delta_{HF} \quad (3)$$

For the monomers, the experimental ionization potentials were taken from NIST. They are 13.778 ± 0.002 eV for CO_2 and 12.5 ± 0.1 eV for SO_2.

Results and discussion

The first section below presents the Molecular Electrostatic Potentials (MEP) of the monomers, which play an instrumental role in guiding the complexes into their optimized geometries. The succeeding sections detail the results first for the CO_2:SO_2 heterodimers, next for the CO_2:$(SO_2)_2$ and $(CO_2)_2$:SO_2 heterotrimers, and finally, for the CO_2:$(SO_2)_3$ and $(CO_2)_3$:SO_2 heterotetramers.

Molecular electrostatic potential (MEP) of the monomers

Carbon dioxide (CO_2) and sulfur dioxide (SO_2) monomers adopt $D_{\infty h}$ and C_{2v} optimized geometries, respectively. MEP at the ±0.020 au contour of each molecule is illustrated in Fig. 1, where red regions correspond to negative potentials and blue regions to positive. This potential is negative along the extensions of the

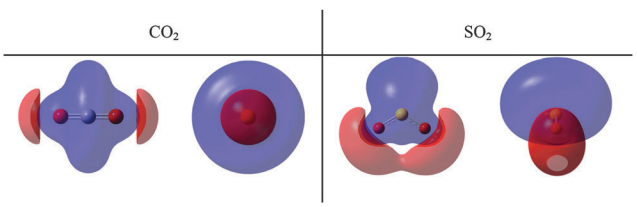

Fig. 1 Molecular Electrostatic Potential (MEP) for the monomers CO_2 and SO_2 at the ±0.020 au contour at the MP2/aug-cc-pVDZ computational level. Lefthand diagram represents molecular plane, and the normal plane is shown on the right. Red and blue regions indicate negative and positive regions, respectively.

C═O bonds of CO_2, and a cylinder of positive potential encircles the central C atom. The potential around the SO_2 molecule is also largely positive with a negative lobe along the extension of each S═O bond. There is a prominent lobe of positive potential above and below the S atom, perpendicular to the molecular plane. The regions of positive potential in CO_2 and SO_2 can be described as π-holes about the central atom, which has its maximum of 37.5 kcal mol^{-1} for CO_2 and 31.2 kcal mol^{-1} for SO_2. These areas represent candidate-binding sites for interactions with the negative potentials of partner molecules. Another perspective on the MEP is that computed on an isodensity surface, displayed in Fig. S1 of the (ESI†), calculated by the WFA-SAS program.[78]

CO_2:SO_2 heterodimers

CO_2 and SO_2 engage in two different minima, illustrated in Fig. 2. The first and more stable one, **A1** with C_{2v} symmetry, has been previously described in the literature by experimental techniques.[79] The second one, **A2** with C_s symmetry, has not been noted in the past even though its energy is very similar to that of **A1**: within around 0.3 kcal mol^{-1} at both the MP2 and CCSD(T) computational levels. As can be seen in Table 1, the interaction energies (E_{int}) at the MP2/aug-cc-pVDZ level are equal to −1.71 and −1.44 kcal mol^{-1}, respectively for **A1** and **A2**, following counterpoise correction of Basis Set Superposition Error (BSSE). These quantities rise slightly to −2.14 and −1.88 kcal mol^{-1} when the CCSD(T) approach is applied to the MP2 geometries. Very similar values can be seen in Table 1 for the binding energies (E_b), indicating very little deformation of the monomer geometries within the complex. Table 2 gathers the various thermodynamic quantities for the association reactions in the CO_2:SO_2 heterodimers at room temperature (298 K). In both cases, ΔS° is negative,

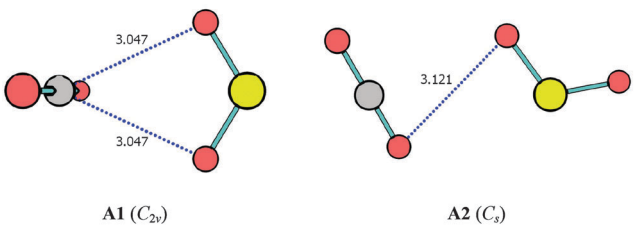

Fig. 2 CO_2:SO_2 heterodimers optimized at the MP2/aug-cc-pVDZ computational level. Blue dotted lines link atoms which present interatomic AIM BCPs, with interatomic distances in Å. Complexes are arranged in ascending order of energy.

Table 1 Interaction (E_{int}) and binding (E_b) energies in kcal mol^{-1} for the CO_2:SO_2 heterodimers at MP2/aug-cc-pVDZ and at CCSD(T)/aug-cc-pVTZ (single point) computational levels

	MP2		CCSD(T)	
Complex	E_{int}[a] (CC)	E_b[b] (ZPE)	E_{int}[a] (CC)	E_b
A1	−2.81 (−1.71)	−2.80 (−2.34)	−2.66 (−2.14)	−2.59
A2	−2.54 (−1.44)	−2.52 (−2.12)	−2.34 (−1.88)	−2.28

[a] In parenthesis, counterpoise correction of the Basis Set Superposition Error (BSSE). [b] In parenthesis, Zero Point Energy (ZPE) addition.

Table 2 Entropy (S) in cal mol^{-1} K^{-1}, enthalpy and Gibbs free energies (H and G) in kcal mol^{-1}, for the association reactions in the CO_2:SO_2 heterodimers at the MP2/aug-cc-pVDZ computational level at room temperature (298 K)

Complex	ΔS	ΔH	ΔG
A1	−20.04	−1.88	4.09
A2	−17.60	−1.61	3.63

as expected for an association reaction. When combined with a slightly negative ΔH°, the free energy of formation becomes positive at 298 K. It is interesting that the less negative value of ΔS° for **A2** as compared to **A1** overrides its less negative ΔH°, leading to a less positive ΔG° at 298 K. A similar stability reversal was observed previously for complexes of SO_2 with H_2CO and H_2CS.

In order to check the reliability of the aug-cc-pVDZ basis set, the structures of **A1** and **A2** were reoptimized with the larger aug-cc-pVTZ set. Only very minor changes in geometry were observed: The R(C···O) distances in **A1** were slightly elongated by 0.040 Å, and R(O···O) in **A2** contracted by 0.008 Å.

Both **A1** and **A2** are consistent with simple Coulombic interactions. **A1** permits the negative regions about the SO_2 O atoms to approach the positive belt that encircles the CO_2 molecule. One of the SO_2 O atoms again overlaps with this positive CO_2 belt in **A2**, but a second attraction, albeit less direct, occurs between the negative potential of the CO_2 O atom and the positive region around the S of SO_2.

Within the context of AIM theory, **A1** presents two symmetrical interactions with bond paths that link the C atom of CO_2 and the O atoms of SO_2, with R(C···O) = 3.047 Å. **A2** is stabilized by a bond path between two O atoms, one on each molecule. These two O atoms are separated by 3.121 Å.

An alternate description of the bonding pattern arises from NBO analysis which emphasizes interorbital interactions. Table 3 and Fig. 3 summarize the important contributions *via* second-order perturbation energies $E(2)$. The pair of symmetrical interactions in **A1** are described in terms of charge transfers from the lone pairs of the O atom to a π* antibonding CO orbital of CO_2. Each such interaction amounts to a value of $E(2)$ equal to 0.83 kcal mol^{-1}. The O···O bond that AIM predicts for **A2**, appears in NBO as a pair of different sorts of interactions. In the first, and stronger interaction, charge is transferred from the SO_2 O lone pair to a π* antibond of CO_2. This contribution of 1.41 kcal mol^{-1} is supplemented by a transfer in the opposite direction, from the O lone pair of CO_2 to a

Table 3 Second-order perturbation NBO energy $E(2)$, in kcal mol^{-1}, for the CO_2:SO_2 heterodimers at the ωB97XD/aug-cc-pVDZ computational level

Complex	Donor/acceptor	Type	$E(2)$
A1	SO_2/CO_2	O_{lp} → π*(CO)	0.83
	SO_2/CO_2	O_{lp} → π*(CO)	0.83
A2	SO_2/CO_2	O_{lp} → π*(CO)	1.41
	CO_2/SO_2	O_{lp} → σ*(SO)	0.37

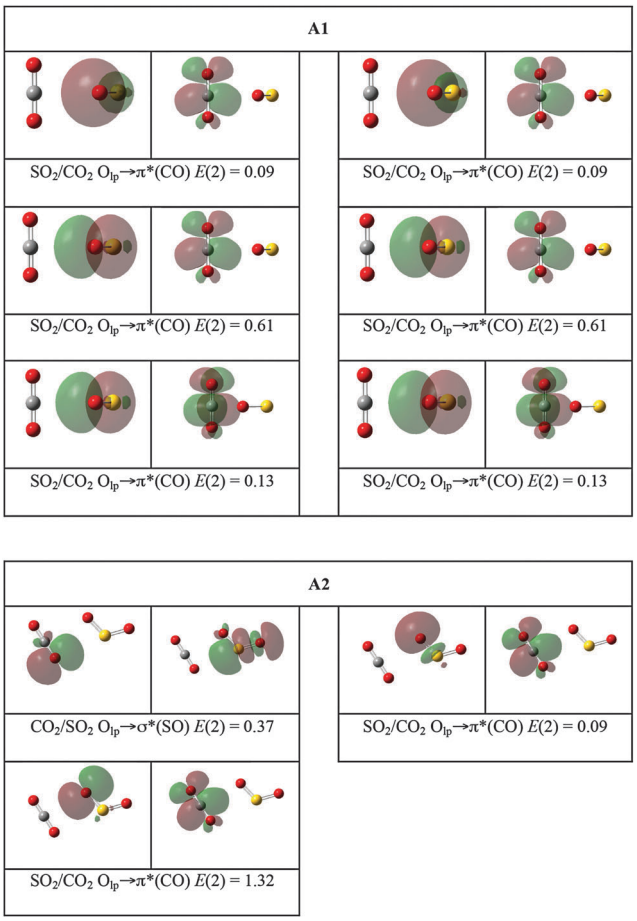

Fig. 3 Orbital interactions (NBO, isovalue ±0.020 au) for the CO_2:SO_2 heterodimers at DFT ωB97XD/aug-cc-pVDZ computational level. $E(2)$ in kcal mol^{-1}.

π* antibond of SO_2, which amounts to 0.37 kcal mol^{-1}. The specific shapes of the involved orbitals are illustrated in Fig. 3, which also partitions the totals in Table 3 into contributions from individual lone pairs and π* orbitals.

Decomposition of the total interaction energy into individual components opens another window into the nature of the interaction. These components, displayed in Table 4, show that the repulsive exchange term is largest, in absolute terms, with values of 3.89 and 3.65 kcal mol^{-1} for **A1** and **A2**, respectively. The attractive electrostatic and dispersion terms are quite similar to one another, between −2.44 and −2.88 kcal mol^{-1}. Induction energy is an order of magnitude smaller, and δ_{HF} even smaller. The two configurations have nearly identical electrostatic and induction energy, so the slightly greater stability of **A1** *vs.* **A2** may be traced to its larger dispersion energy.

As two molecules begin to approach and interact with one another, they perturb one another's electron clouds. The shifts

Table 4 Interaction energy terms in kcal mol^{-1} for the CO_2:SO_2 complexes, calculated using the DFT-SAPT (PBE0/aug-cc-pVTZ) methodology

Complex	E_{ele}	E_{exc}	E_{ind}	E_{dis}	δ_{HF}	$E^{DFT\text{-}SAPT}$
A1	−2.68	3.89	−0.24	−2.88	−0.13	−2.03
A2	−2.55	3.65	−0.33	−2.44	−0.15	−1.82

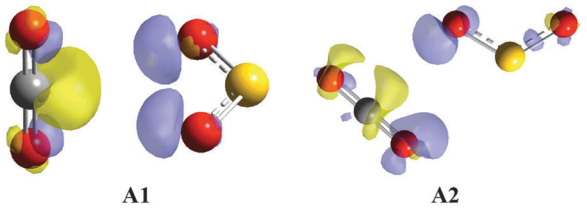

Fig. 4 Electron Density Shifts (EDS) occurring within CO_2:SO_2 heterodimers at MP2/aug-cc-pVDZ level. Blue and yellow colors refer to gain and loss of density in complex, respectively, relative to isolated monomers. Isosurface value ±0.0005 au.

in total electron density that occur as a result of the formation of each complex are illustrated in Fig. 4, where blue and yellow regions indicate respective gains and losses of density, relative to the isolated monomers. In both heterodimers, there is a loss of density near the C atom, facing SO_2. This pattern is consistent with the NBO interpretation of involvement of O lone pairs with CO π* antibonds. The O atoms of SO_2 that interact with CO_2 show a density gain, as does the O atom of CO_2 in **A2** that interacts with SO_2.

The redistribution patterns in Fig. 4 provide an interesting alternative view of the electron density to the AIM picture in Fig. 2. In the case of **A1**, the two AIM C···O bonds are reflected by a shift of density from C to O, C losing density and O gaining. In contrast, both of the O atoms involved in the AIM O···O bond of **A2** gain density. The latter may perhaps be explained in part by the NBO view of the bonding which is dual in nature. There is first of all the transfer from the O lone pair of SO_2 to π* of CO_2, chiefly involving the O atom of SO_2 which is involved in the AIM bond. (Notably, the O atom from CO_2 which participates in this bond is not involved in the recipient CO_2 π* orbital, see Fig. 3.) As a second component, there is also a transfer in the reverse direction, from an O lone pair of CO_2 to a σ* orbital of SO_2. This transfer involves the O atom of CO_2 that does participate in this same AIM bond (but not the participating O atom from SO_2). So, the density shift in Fig. 4 may be thought of as the sum of two separate processes, each of which separately account for the change observed in the two O atoms involved in the AIM O···O bond of **A2**.

Heterotrimers

Minimum-energy configurations for the mixed $(CO_2)_2$:SO_2 and CO_2:$(SO_2)_2$ heterotrimers were identified following a dual strategy: (i) inserting the third molecule (CO_2 and SO_2 in each case) in various locations around the aforementioned CO_2:SO_2 optimized dimers, taking into account their MEP; and (ii) fresh starting points, with no prejudice toward the heterodimer structures.

(i) $(CO_2)_2$:SO_2 heterotrimers. The structures of the $(CO_2)_2$:SO_2 heterotrimers optimized at the MP2/aug-cc-pVDZ computational level are gathered in Fig. 5. A total of 4 unique minima have been obtained (**B1** to **B4**), with all of them derived in some sense from the **A1** or **A2** heterodimers, *i.e.*, a principal geometrical disposition between the CO_2 and the SO_2 monomers noted in the heterodimers remains in these $(CO_2)_2$:SO_2 structures. Specifically, in **B1**, **B2**, and **B3**, the SO_2 molecule is poised with its two O atoms

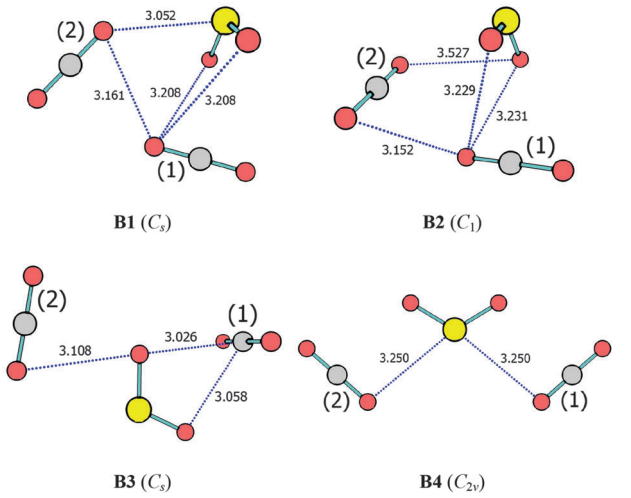

Fig. 5 $(CO_2)_2$:SO_2 heterotrimers optimized at MP2/aug-cc-pVDZ computational level. Broken blue lines link atoms which present interatomic AIM BCPs, with interatomic distances in Å. Complexes are arranged in ascending order of energy.

roughly symmetrically disposed around $CO_2(1)$. One difference appears in the AIM analysis of **B1** and **B2**, which places bonds between O atoms, not the C···O of **A1**. The O···O interaction that characterizes **A2** is present in **B2** and **B3** in terms of $CO_2(2)$. The noncyclic **B4** geometry places the SO_2 in the center, such that the two CO_2 molecules are situated very similarly to **A2**, although the AIM treatment of the electron density topology describes O···S bonds, rather than the O···O of **A2**. The second CO_2 molecule in noncyclic **B3** also interacts with the central SO_2 much as it does in **A2**.

It is notable that there are no minima present in which the two CO_2 monomers interact directly with one another. This absence can be attributed to the weak forces between CO_2 molecules: the most stable T-shape CO_2 dimer[80] has an interaction energy of -1.11 kcal mol^{-1} at the counterpoise-corrected CCSD(T)/aug-cc-pVTZ//MP2/aug-cc-pVDZ level, roughly half of that for the mixed CO_2:SO_2 heterodimer.

The interaction energies and the pairwise energies derived from the multi-body analysis of these heterotrimers are reported in Table 5. The first point to note is that the pairwise terms are little changed from the interactions in the dimers. Specifically, the MP2/aug-cc-pVDZ interaction energies for **A1** and **A2** in Table 1 are -2.81 and -2.54 kcal mol^{-1}, respectively. The former value is nearly duplicated for E_{12} in **B1**, **B2**, and **B3**, where the SO_2 and $CO_2(1)$ molecules are disposed much as in **A1**.

Table 5 Multi-body energy terms in kcal mol^{-1} for the $(CO_2)_2$:SO_2 heterotrimers at MP2/aug-cc-pVDZ computational level. Subscripts 1, 2 and 3 refer to $CO_2(1)$, SO_2 and $CO_2(2)$ molecules in the heterotrimer complexes (see Fig. 5)

Complex	E_{12}	E_{13}	E_{23}	$\Sigma\Delta^2E$	Σ^3E	Total E_{int}
B1	−2.83	−1.56	−2.23	−6.62	−0.23	−6.85
B2	−2.82	−1.35	−2.44	−6.61	−0.21	−6.82
B3	−2.83	−0.06	−2.57	−5.46	0.02	−5.44
B4	−2.54	−0.05	−2.55	−5.14	0.05	−5.09

Likewise, E_{23}, which reflects the interaction between SO_2 and $CO_2(2)$, is rather close to -2.54 kcal mol^{-1} in all four cases, as is E_{12} in **B4**, reflecting the similar configuration as in **A2**. As **B3** and **B4** are noncyclic, the two CO_2 molecules are far apart, which results in a near zero value of E_{13}. In contrast, the closer approach of these two molecules in **B1** and **B2** results in a pairwise attraction of -1.56 and -1.35 kcal mol^{-1}, respectively. It is this latter $CO_2\cdots CO_2$ attraction which is primarily responsible for the greater stability of these two cyclic trimers, along with a small cooperative Σ^3E attraction up to -0.23 kcal mol^{-1}.

Table S1 (ESI†) summarizes the NBO analysis for the $(CO_2)_2$:SO_2 heterotrimers. The $O_{lp} \rightarrow \pi^*(CO)$ interactions of **A1** remain in **B1**, **B2**, and **B3**, and in roughly equal measure. Similarly, the $O_{lp} \rightarrow \pi^*(CO)$ transfer of **A2** is reproduced in **B3** and **B4**, also with little diminution in its value. New interactions arise in **B1** and **B2**. Both of these structures contain an $O_{lp} \rightarrow \pi^*(CO)$ transfer involving the two CO_2 molecules, consistent with the O···O AIM bond in Fig. 5, with R(O···O) ∼ 3.15 Å. The attractive force between SO_2 and $CO_2(2)$ can be traced to an $O_{lp} \rightarrow \pi^*(SO)$ transfer, an interaction that is not seen in any dimers. It is interesting that this same $O_{lp} \rightarrow \pi^*(SO)$ transfer, and in equal amounts, is characterized by AIM as an O···S bond in **B1**, but an O···O bond in **B2**.

(ii) CO_2:$(SO_2)_2$ heterotrimers. The 11 unique minima of the CO_2:$(SO_2)_2$ heterotrimer optimized at the MP2/aug-cc-pVDZ computational level are gathered in Fig. 6. **C1** to **C8** may all be

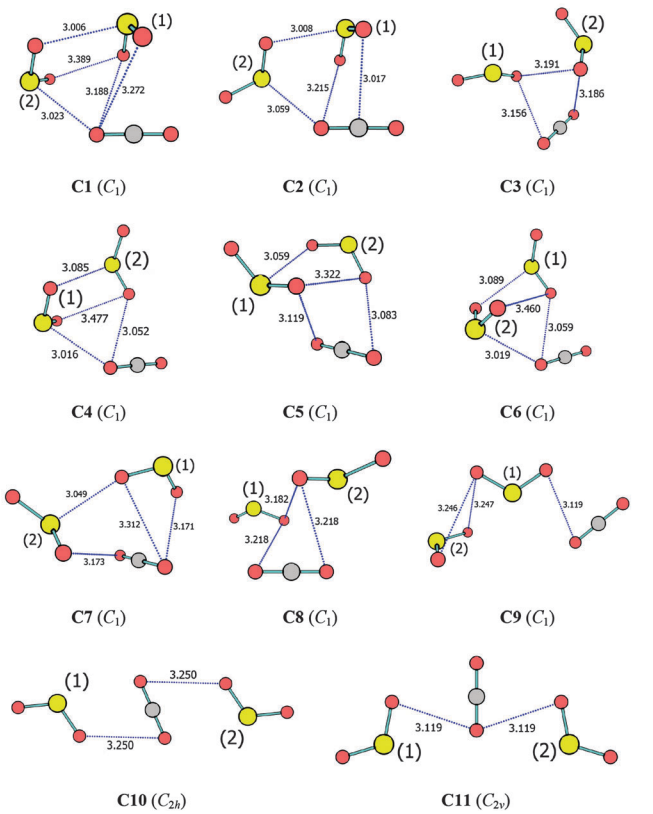

Fig. 6 CO_2:$(SO_2)_2$ heterotrimers optimized at the MP2/aug-cc-pVDZ level. Blue broken lines link atoms which present interatomic AIM BCPs, with interatomic distances in Å. Complexes are arranged in ascending order of energy.

Table 6 Multi-body energy terms in kcal mol^{-1} for the CO_2:$(SO_2)_2$ heterotrimers at MP2/aug-cc-pVDZ computational level. Subscripts 1, 2 and 3 refer to CO_2(1), SO_2 and CO_2(2) molecules in the heterotrimer complexes (see Fig. 6)

Complex	E_{12}	E_{13}	E_{23}	$\Sigma\Delta^2E$	Δ^3E	Total E_{int}
C1	−2.83	−2.17	−3.15	−8.15	−0.45	−8.60
C2	−2.83	−1.78	−3.48	−8.09	−0.37	−8.46
C3	−2.23	−2.10	−3.70	−8.03	−0.10	−8.13
C4	−2.16	−2.06	−3.42	−7.64	−0.40	−8.04
C5	−2.53	−1.88	−3.30	−7.71	−0.15	−7.86
C6	−2.07	−2.16	−3.14	−7.37	−0.37	−7.74
C7	−2.60	−2.17	−2.74	−7.51	0.00	−7.51
C8	−2.17	−2.17	−3.01	−7.35	−0.09	−7.44
C9	−2.56	−0.08	−3.75	−6.39	0.04	−6.35
C10	−2.51	−2.51	−0.24	−5.27	−0.04	−5.30
C11	−2.55	−2.55	0.10	−4.99	−0.17	−5.16

classified as cyclic, and the three higher-energy trimers are linear. In order to understand the reasons underlying their geometries, it must first be pointed out that $(SO_2)_2$ dimers[81] are more strongly bound than are the mixed SO_2:CO_2 heterodimer. There are three different $(SO_2)_2$ configurations, displayed in Fig. S2 (ESI†), and as reported in Table S2 (ESI†), their interaction energies vary between 2.52 and 3.02 kcal mol^{-1}, larger than the 1.88–2.14 kcal mol^{-1} range of the heterodimer at the same CCSD(T) level. It is thus the preferred $SO_2\cdots SO_2$ intermolecular arrangements which play a dominant role in the CO_2:$(SO_2)_2$ heterotrimers. For example, the most stable **C1** structure resembles the lowest energy $(SO_2)_2$ dimer in terms of the arrangement of the two SO_2 molecules, as does **C2–C4**. Nonetheless, one can see remnants of the preferred heterodimer arrangements within the structures of Fig. 6. For example, the **A1** configuration is evident within **C1** and **C2**, and **C9–C11** are reminiscent of **A2**.

The interaction energies and the pairwise energies derived from the multi-body analysis of these heterotrimers are reported in Table 6. The cyclic structures **C1–C8** are bound by between 7.44 and 8.60 kcal mol^{-1}, and the remaining linear geometries by between 5.16 and 6.35 kcal mol^{-1}. Consistent with the strong binding between SO_2 molecules, it is E_{23} which is generally the largest term in Table 6. E_{12}, comprising the interaction between CO_2 and a SO_2 molecule, is equal to −2.83 kcal mol^{-1} for **C1** and **C2**, the same as in the simple CO_2:SO_2 **A1** dimer. Similarly, this same quantity is 2.51–2.56 kcal mol^{-1} in **C9–C11** which is equal to ΔE for **A2**. Structures **C1–C6** exhibit the most negative three-body Δ^3E term, corresponding to the strongest cooperativity. This quantity is much smaller in the linear geometries **C9–C11**.

Table S3 of the ESI† contains the NBO analysis for the CO_2:$(SO_2)_2$ heterotrimers. The SO_2 molecules interact with one another primarily *via* $O_{lp} \rightarrow \pi^*(SO)$ and $\pi(SO) \rightarrow \pi^*(SO)$ transfers, although **C5** contains elements of an $O_{lp} \rightarrow \sigma^*(SO)$ transfer. Interactions between SO_2 and CO_2 are largely a repeat of those seen in the SO_2:$(CO_2)_2$ heterotrimers, namely $O_{lp} \rightarrow \pi^*(CO)$, and some of the reverse $O_{lp} \rightarrow \pi^*(SO)$. There is a new transfer, only in **C6**, from the O lone pair of SO_2 to a "lone vacant" C orbital of CO_2. $E(2)$ for this transfer is surprisingly large, at 2.02 kcal mol^{-1}. It is notable that this C$\cdots$O interaction is not reflected by a corresponding bond in the AIM analysis of this structure.

Heterotetramers

Minima for 1 : 3 and 3 : 1 heterotetramers were searched taking as starting points the optimized heterotrimer structures. An exhaustive search yielded 16 (**D1–D16**) and 38 (**E1–E38**) different minima for the $(CO_2)_3$:SO_2 and CO_2:$(SO_2)_3$ heterotetramers, respectively. The 16 $(CO_2)_3$:SO_2 heterotetramers span an energy range of 4.98 kcal mol^{-1}, with total interaction energies between −6.98 and −11.95 kcal mol^{-1}. The CO_2:$(SO_2)_3$ structures span a slightly wider range of 6.64 kcal mol^{-1}, and are more strongly bound, varying between −9.12 and −15.76 kcal mol^{-1}.

Fig. S3 and S4 (ESI†) display the most stable minima of each type, with energies within 1 kcal mol^{-1} of one another. As reported in these figures and Tables S4 and S5 (ESI†), there are 3 such structures for $(CO_2)_3$:SO_2 with similar energies and 10 for CO_2:$(SO_2)_3$. Examination of these structures reveals that the **D1** and **D3** minima may be thought of as combining elements of the **A1** CO_2:SO_2 heterodimer and the **B1** and **B2** $(CO_2)_2$:SO_2 heterotrimers, respectively. **D2**, on the other hand, has little resemblance to the prior dimer and trimer structures. All ten of the lowest-energy CO_2:$(SO_2)_3$ heterotetramers have one feature in common. The three SO_2 molecules form a ring, a sort of "SO_2-wheel", to which the CO_2 is attached.

Examination of Tables S4 and S5 (ESI†) reveals that the cooperativity effects are minimal at the four-body level, with Δ^4E less than 0.06 and 0.11 kcal mol^{-1} for $(CO_2)_3$:SO_2 and CO_2:$(SO_2)_3$ heterotetramers, respectively. Three-body effects are much larger in these complexes than in the heterotrimers, with $-\Delta^3E$ as high as 0.59 and 1.29 kcal mol^{-1} for $(CO_2)_3$:SO_2 and CO_2:$(SO_2)_3$, respectively, in comparison to only 0.23 and 0.45 kcal mol^{-1} for their $(CO_2)_2$:SO_2 and CO_2:$(SO_2)_2$ trimer counterparts. It is tempting to speculate that this cooperativity will continue to grow as the system approaches the situation approximating CO_2 dissolved in SO_2 solvent, or *vice versa*.

Summary and conclusions

The CO_2:SO_2 heterodimer exists in two stable structures, both bound by about 2 kcal mol^{-1}. The more stable of the two belongs to the C_{2v} point group, with the two O atoms of SO_2 symmetrically disposed above and below the C atom of CO_2. While AIM analysis leads to the idea of a pair of C$\cdots$O bonds, NBO treatment describes the bonding in terms of charge transfer from O lone pairs to the CO π^* antibonding orbitals. The geometry of the slightly less stable structure places one of the S–O bonds parallel to the OCO molecule. The AIM model of an O$\cdots$O chalcogen bond contrasts with the NBO version which retains the $O_{lp} \rightarrow \pi^*(CO)$ transfer of the global minimum, supplemented by transfer in the opposite direction from the O lone pair of CO_2 to a π^* antibond of SO_2. Electron redistribution patterns are supportive of the NBO interpretation of the bonding. Both structures are consonant with attractions between oppositely charged regions of the molecular electrostatic potentials of the two monomers. Decomposition of the interaction energies points to electrostatic attraction and dispersion as the dominant attractive components, in roughly equal measure.

The various heterotrimers derived by adding either a CO_2 or SO_2 molecule to the heterodimer generally retain the dimer structure as a starting point. Due to the stronger interaction between pairs of SO_2 as compared to CO_2 molecules, the $(SO_2)_2$:CO_2 trimers are more strongly bound than $(CO_2)_2$:SO_2. In general, the most stable of the various heterotrimer structures are cyclic in that all three molecules interact directly with one another. In the case of the less stable linear trimers, it is SO_2 rather than CO_2 that tends toward the central position. The trimers present an interaction not observed in the dimers, the charge transfer from the lone pairs of a CO_2 O atom to the π^* S–O antibonding orbital. Multi-body analysis suggests that cooperativity is fairly small in these heterotrimers, less than 0.5 kcal mol^{-1}. The number of minima continues to increase as a fourth molecule is added, with 16 structures identified for $(CO_2)_3$:SO_2 and 38 for CO_2:$(SO_2)_3$. The most strongly bound, of the latter category, has a total interaction energy of 16 kcal mol^{-1}. Four body effects are quite small, although the total three-body energies are as large as 1.3 kcal mol^{-1}.

Acknowledgements

LMA thanks the MICINN for a PhD grant (No. BES-2010-031225), the MINECO (Project No. CTQ2012-35513-C02-02) and the Comunidad Autónoma de Madrid (Project MADRISOLAR2, ref. S2009/PPQ-1533) for continuing support. Computer, storage and other resources from the Division of Research Computing in the Office of Research and Graduate Studies at Utah State University and the CTI (CSIC) are gratefully acknowledged. Gratitude is also due to Prof. Ibon Alkorta from IQM-CSIC, for the NBO analysis with the NBO6.0 program.

References

1 P. Schuster, G. Zundel and C. Sandorfy, *The Hydrogen Bond. Recent Developments in Theory and Experiments*, North-Holland Publishing Co., Amsterdam, Netherlands, 1976.
2 S. Scheiner, *Hydrogen Bonding: A Theoretical Perspective*, Oxford University Press, New York, USA, 1997.
3 S. J. Grabowski, *Hydrogen Bonding - New Insights*, Springer, Dordrecht, Netherlands, 2006.
4 G. Gilli and P. Gilli, *The Nature of the Hydrogen Bond*, Oxford University Press, Oxford, UK, 2009.
5 A. Bhattacherjee, Y. Matsuda, A. Fujii and S. Wategaonkar, *ChemPhysChem*, 2013, **14**, 905–914.
6 K. Grzechnik, K. Rutkowski and Z. Mielke, *J. Mol. Struct.*, 2012, **1009**, 96–102.
7 H. S. Biswal and S. Wategaonkar, *J. Phys. Chem. A*, 2009, **113**, 12774–12782.
8 D. Mani and E. Arunan, *Phys. Chem. Chem. Phys.*, 2013, **15**, 14377–14383.
9 E. Arunan, G. R. Desiraju, R. A. Klein, J. Sadlej, S. Scheiner, I. Alkorta, D. C. Clary, R. H. Crabtree, J. J. Dannenberg, P. Hobza, H. G. Kjaergaard, A. C. Legon, B. Mennucci and D. J. Nesbitt, *Pure Appl. Chem.*, 2011, **83**, 1619–1636.
10 M. Saggu, N. M. Levinson and S. G. Boxer, *J. Am. Chem. Soc.*, 2012, **134**, 18986–18997.
11 M. Nishio, *Phys. Chem. Chem. Phys.*, 2011, **13**, 13873–13900.
12 B. G. d. Oliveira, *Phys. Chem. Chem. Phys.*, 2013, **15**, 37–79.
13 O. Takahashi, Y. Kohno and M. Nishio, *Chem. Rev.*, 2010, **110**, 6049–6076.
14 T. Nakanaga, K. Buchhold and F. Ito, *Chem. Phys.*, 2003, **288**, 69–76.
15 T. Kar and S. Scheiner, *J. Chem. Phys.*, 2003, **119**, 1473–1482.
16 P. C. Singh and G. Naresh Patwari, *Chem. Phys. Lett.*, 2006, **419**, 265–268.
17 N. V. Belkova, E. S. Shubina and L. M. Epstein, *Acc. Chem. Res.*, 2005, **38**, 624–631.
18 M. Solimannejad and S. Scheiner, *J. Phys. Chem. A*, 2005, **109**, 11933–11935.
19 J. P. M. Lommerse, A. J. Stone, R. Taylor and F. H. Allen, *J. Am. Chem. Soc.*, 1996, **118**, 3108–3116.
20 P. Metrangolo and G. Resnati, *Science*, 2008, **321**, 918–919.
21 W. Zierkiewicz, D. Michalska and T. Zeegers-Huyskens, *Phys. Chem. Chem. Phys.*, 2010, **12**, 13681–13691.
22 U. Adhikari and S. Scheiner, *Chem. Phys. Lett.*, 2012, **532**, 31–35.
23 P. Politzer, J. Murray and M. Concha, *J. Mol. Model.*, 2008, **14**, 659–665.
24 P. Hobza and K. Müller-Dethlefs, *Non-Covalent Interactions*, The Royal Society of Chemistry, Cambridge, UK, 2009.
25 R. E. Rosenfield, R. Parthasarathy and J. D. Dunitz, *J. Am. Chem. Soc.*, 1977, **99**, 4860–4862.
26 F. T. Burling and B. M. Goldstein, *J. Am. Chem. Soc.*, 1992, **114**, 2313–2320.
27 D. B. Werz, R. Gleiter and F. Rominger, *J. Am. Chem. Soc.*, 2002, **124**, 10638–10639.
28 M. Iwaoka, S. Takemoto and S. Tomoda, *J. Am. Chem. Soc.*, 2002, **124**, 10613–10620.
29 C. Bleiholder, D. B. Werz, H. Köppel and R. Gleiter, *J. Am. Chem. Soc.*, 2006, **128**, 2666–2674.
30 G. Sánchez-Sanz, I. Alkorta and J. Elguero, *Mol. Phys.*, 2011, **109**, 2543–2552.
31 M. A. Jabłoński, *J. Phys. Chem. A*, 2012, **116**, 3753–3764.
32 R. D. Chapman, R. D. Gilardi, M. F. Welker and C. B. Kreutzberger, *J. Org. Chem.*, 1999, **64**, 960–965.
33 U. Adhikari and S. Scheiner, *Chem. Phys. Lett.*, 2012, **536**, 30–33.
34 S. Tschirschwitz, P. Lonnecke and E. Hey-Hawkins, *Dalton Trans.*, 2007, 1377–1382, DOI: 10.1039/b617257a.
35 S. Scheiner, *J. Phys. Chem. A*, 2011, **115**, 11202–11209.
36 M. Bühl, P. Kilian and J. D. Woollins, *ChemPhysChem*, 2011, **12**, 2405–2408.
37 S. Scheiner, *Acc. Chem. Res.*, 2012, **46**, 280–288.
38 J. S. Murray, P. Lane and P. Politzer, *Int. J. Quantum Chem.*, 2007, **107**, 2286–2292.
39 A. Mohajeri, A. H. Pakiari and N. Bagheri, *Chem. Phys. Lett.*, 2009, **467**, 393–397.
40 I. Alkorta, G. Sánchez-Sanz, J. Elguero and J. E. Del Bene, *J. Chem. Theory Comput.*, 2012, **8**, 2320–2327.
41 G. Sanchez-Sanz, C. Trujillo, M. Solimannejad, I. Alkorta and J. Elguero, *Phys. Chem. Chem. Phys.*, 2013, **15**, 14310–14318.

42 J. Murray, P. Lane and P. Politzer, *J. Mol. Model.*, 2009, **15**, 723–729.
43 P. Politzer, J. S. Murray and T. Clark, *Phys. Chem. Chem. Phys.*, 2013, **15**, 11178–11189.
44 P. G. Taylor, A. R. Bassindale, Y. El Aziz, M. Pourny, R. Stevenson, M. B. Hursthouse and S. J. Coles, *Dalton Trans.*, 2012, **41**, 2048–2059.
45 A. Bauzá, T. J. Mooibroek and A. Frontera, *Angew. Chem., Int. Ed.*, 2013, **52**, 12317–12321.
46 J. Murray, P. Lane, T. Clark, K. Riley and P. Politzer, *J. Mol. Model.*, 2012, **18**, 541–548.
47 U. Adhikari and S. Scheiner, *J. Phys. Chem. A*, 2012, **117**, 489–496.
48 A. Choudhary, C. G. Fry, K. J. Kamer and R. T. Raines, *Chem. Commun.*, 2013, **49**, 8166–8168.
49 W. H. J. Iii, E. G. Buchanan, C. W. Müller, J. C. Dean, D. Kosenkov, L. V. Slipchenko, L. Guo, A. G. Reidenbach, S. H. Gellman and T. S. Zwier, *J. Phys. Chem. A*, 2011, **115**, 13783–13798.
50 C. E. Jakobsche, A. Choudhary, S. J. Miller and R. T. Raines, *J. Am. Chem. Soc.*, 2010, **132**, 6651–6653.
51 U. Adhikari and S. Scheiner, *ChemPhysChem*, 2012, **13**, 3535–3541.
52 G. J. Bartlett, A. Choudhary, R. T. Raines and D. N. Woolfson, *Nat. Chem. Biol.*, 2010, **6**, 615–620.
53 L. M. Azofra and S. Scheiner, *J. Chem. Phys.*, 2014, **140**, 034302.
54 T. R. Karl and K. E. Trenberth, *Science*, 2003, **302**, 1719–1723.
55 C. Capello, U. Fischer and K. Hungerbuhler, *Green Chem.*, 2007, **9**, 927–934.
56 V. K. Potluri, J. Xu, R. Enick, E. Beckman and A. D. Hamilton, *Org. Lett.*, 2002, **4**, 2333–2335.
57 M. Altarsha, V. Yeguas, F. Ingrosso, R. López and M. F. Ruiz-López, *J. Phys. Chem. B*, 2013, **117**, 3091–3097.
58 M. Altarsha, F. Ingrosso and M. F. Ruiz-Lopez, *ChemPhysChem*, 2012, **13**, 3397–3403.
59 L. Azofra, M. Altarsha, M. Ruiz-López and F. Ingrosso, *Theor. Chem. Acc.*, 2013, **132**, 1–9.
60 G. E. Likens and F. H. Bormann, *Science*, 1974, **184**, 1176–1179.
61 J. G. Calvert, A. Lazrus, G. L. Kok, B. G. Heikes, J. G. Walega, J. Lind and C. A. Cantrell, *Nature*, 1985, **317**, 27–35.
62 C. Møller and M. S. Plesset, *Phys. Rev.*, 1934, **46**, 618–622.
63 T. H. Dunning Jr., *J. Chem. Phys.*, 1989, **90**, 1007–1023.
64 D. E. Woon and T. H. Dunning Jr., *J. Chem. Phys.*, 1994, **100**, 2975–2988.
65 D. E. Woon and T. H. Dunning Jr., *J. Chem. Phys.*, 1995, **103**, 4572–4585.
66 T. H. Dunning, *J. Chem. Phys.*, 1989, **90**, 1007–1023.
67 J. A. Pople, M. Head-Gordon and K. Raghavachari, *J. Chem. Phys.*, 1987, **87**, 5968–5975.
68 M. J. Frisch, G. W. Trucks, H. B. Schlegel, G. E. Scuseria, M. A. Robb, J. R. Cheeseman, G. Scalmani, V. Barone, B. Mennucci, G. A. Petersson, H. Nakatsuji, M. Caricato, X. Li, H. P. Hratchian, A. F. Izmaylov, J. Bloino, G. Zheng, J. L. Sonnenberg, M. Hada, M. Ehara, K. Toyota, R. Fukuda, J. Hasegawa, M. Ishida, T. Nakajima, Y. Honda, O. Kitao, H. Nakai, T. Vreven, J. A. Montgomery, Jr., J. E. Peralta, F. Ogliaro, M. Bearpark, J. J. Heyd, E. Brothers, K. N. Kudin, V. N. Staroverov, R. Kobayashi, J. Normand, K. Raghavachari, A. Rendell, J. C. Burant, S. S. Iyengar, J. Tomasi, M. Cossi, N. Rega, N. J. Millam, M. Klene, J. E. Knox, J. B. Cross, V. Bakken, C. Adamo, J. Jaramillo, R. Gomperts, R. E. Stratmann, O. Yazyev, A. J. Austin, R. Cammi, C. Pomelli, J. W. Ochterski, R. L. Martin, K. Morokuma, V. G. Zakrzewski, G. A. Voth, P. Salvador, J. J. Dannenberg, S. Dapprich, A. D. Daniels, Ö. Farkas, J. B. Foresman, J. V. Ortiz, J. Cioslowski and D. J. Fox, Gaussian, Inc., Wallingford CT, 2009.
69 S. F. Boys and F. Bernardi, *Mol. Phys.*, 1970, **19**, 553–566.
70 R. F. W. Bader, *Atoms in Molecules: A Quantum Theory*, Clarendon Press, Oxford, UK, 1990.
71 T. A. Keith, *TK Gristmill Software*, Overland Park KS, USA, 2013.
72 F. Weinhold and C. R. Landis, *Valency and Bonding. A Natural Bond Orbital Donor- Aceptor Perspective*, Cambridge Press, Cambridge, UK, 2005.
73 J.-D. Chai and M. Head-Gordon, *Phys. Chem. Chem. Phys.*, 2008, **10**, 6615–6620.
74 E. D. Glendening, J. K. Badenhoop, A. E. Reed, J. E. Carpenter, J. A. Bohmann, C. M. Morales, C. R. Landis and F. Weinhold, NBO6.0, Theoretical Chemistry Institute, University of Wisconsin, Madison, USA, 2013.
75 J. P. Perdew, K. Burke and M. Ernzerhof, *Phys. Rev. Lett.*, 1996, **77**, 3865–3868.
76 H.-J. Werner, P. J. Knowles, F. R. Manby, M. Schütz, P. Celani, G. Knizia, T. Korona, R. Lindh, A. Mitrushenkov, G. Rauhut, T. B. Adler, R. D. Amos, A. Bernhardsson, A. Berning, D. L. Cooper, M. J. O. Deegan, A. J. Dobbyn, F. Eckert, E. Goll, C. Hampel, A. Hesselmann, G. Hetzer, T. Hrenar, G. Jansen, C. Köppl, Y. Liu, A. W. Lloyd, R. A. Mata, A. J. May, S. J. McNicholas, W. Meyer, M. E. Mura, A. Nicklaß, P. Palmieri, K. Pflüger, R. Pitzer, M. Reiher, T. Shiozaki, H. Stoll, A. J. Stone, R. Tarroni, T. Thorsteinsson, M. Wang and A. Wolf, 2012.
77 G. Chałasiński and M. M. Szcześniak, *Chem. Rev.*, 2000, **100**, 4227–4252.
78 F. Bulat, A. Toro-Labbé, T. Brinck, J. Murray and P. Politzer, *J. Mol. Model.*, 2010, **16**, 1679–1691.
79 S. A. Peebles, L. Sun and R. L. Kuczkowski, *J. Chem. Phys.*, 1999, **110**, 6804–6811.
80 K. W. Jucks, Z. S. Huang, D. Dayton, R. E. Miller and W. J. Lafferty, *J. Chem. Phys.*, 1987, **86**, 4341–4346.
81 D. D. Nelson, G. T. Fraser and W. Klemperer, *J. Chem. Phys.*, 1985, **83**, 945–949.